Domain-swapped chain connectivity and gated membrane access in a Fab-mediated crystal of the human TRAAK K^+ channel

Stephen G. Brohawn, Ernest B. Campbell, and Roderick MacKinnon[1]

Laboratory of Molecular Neurobiology and Biophysics and Howard Hughes Medical Institute, The Rockefeller University, New York, NY 10065

Edited by Christopher Miller, Howard Hughes Medical Institute, Brandeis University, Waltham, MA, and approved December 19, 2012 (received for review October 31, 2012)

TRAAK (TWIK-related arachidonic acid-stimulated K^+ channel, K2P4.1) K^+ ion channels are expressed predominantly in the nervous system to control cellular resting membrane potential and are regulated by mechanical and chemical properties of the lipid membrane. TRAAK channels are twofold symmetric, which precludes a direct extension of gating mechanisms that close canonical fourfold symmetric K^+ channels. We present the crystal structure of human TRAAK in complex with antibody antigen-binding fragments (Fabs) at 2.75-Å resolution. In contrast to a previous structure, this structure reveals a domain-swapped chain connectivity enabled by the helical cap that exchanges two opposing outer helices 180° around the channel. An unrelated conformational change of an inner helix seals a side opening to the membrane bilayer and is associated with structural changes around the K^+-selectivity filter that may have implications for mechanosensitivity and gating of TRAAK channels.

ion channel gating | mechanosensitivity | two-pore domain potassium channel

Canonical K^+ channel structures consist of four identical subunits arranged with fourfold symmetry. Recently, structures of the two-pore domain K^+ (K2P) channels TRAAK (TWIK-related arachidonic acid-stimulated K^+ channel) and TWIK-1 (Tandem of P domains in a weak inward rectifying K^+ channel) showed, as expected from their amino acid sequences, that they are twofold symmetric (1, 2). Twofold symmetry arises in these channels because they are formed from two polypeptide chains instead of four, but each chain encodes two nonidentical repeats corresponding to the subunits of a fourfold symmetric channel. This symmetry difference is relevant to understanding their function because gating in canonical K^+ channels, in many cases, is known to involve a fourfold symmetric dilation of the conduction pathway near the intracellular surface (3, 4). The twofold symmetric nature of TRAAK precludes a direct extension of this principle. How then do mechanical deformations of the cell membrane and polyunsaturated fatty acids such as arachidonic acid, which are able to partition into the membrane, regulate gating in the TRAAK K^+ channel (5)? Two additional distinguishing structural features of TRAAK (and TWIK-1) were the presence of an extracellular helical cap and intramembrane lateral openings that expose the ion-conduction pathway directly to the hydrophobic core of the lipid membrane (1, 2). What ramifications these structural features may have on functional properties of these channels remains to be determined.

We raised mouse monoclonal antibodies against the human TRAAK K^+ channel and used an antigen-binding fragment (Fab) from one of these in crystallization. Diffraction data were collected to 2.75-Å Bragg spacings, and the structure was solved by molecular replacement using a Fab search model. The final structure, which consists of one channel and two Fabs in the asymmetric unit, was refined to R_{work}/R_{free} of 20.1/23.6% (Fig. 1*A* and Table S1). The Fabs are bound specifically to the top of the helical cap. The crystal consists of layers of Fabs that contact the channel at the cap and at intracellular extensions of the channel (Fig. S1). Comparison with the original TRAAK structure determined at 3.8-Å resolution [Protein Data Bank (PDB) ID code 3UM7 (1)] leads us to the following two observations: first, two helices are domain-swapped across the channel dimer; and second, there is a conformational difference in one subunit that closes the intramembrane lateral opening and appears to correlate structural changes near the intracellular C terminus with changes near the extracellular surface surrounding the selectivity filter.

During refinement, it was evident that electron density features at the top of the helical cap were inconsistent with the conformation of four amino acids (His^{76}-Val^{79}) in the original model. Rebuilding these four amino acids showed an unexpected yet unambiguous crossover in connectivity, which means the two subunits domain-swapped their outer helix 1-cap helix 1 unit in the crystal structure (i.e., the unit on one subunit exchanged places with its identical copy on the other subunit) (Fig. 1 *B* vs. *C*). This observation is unexpected because in all other K^+ channels of known structure, the outer helix in a subunit interacts with the inner helix from the same subunit (Fig. 1*D*). Because we have never before observed such domain swapping in a K^+ channel, we wondered whether this event could have occurred after extraction from the membrane into detergent. Attempts to address this by crosslinking subunits within the cell membrane using site-directed cysteine mutagenesis yielded ambiguous results. We, thus, appealed to the antibody that was used to crystalize the channel, noting that approximately one-third of the heavy chain-interacting epitope (one-quarter of the entire Fab epitope) on the channel surface involves the very four amino acids in question (His^{76}-Val^{79}) across both channel subunits (Fig. 2*A*). We conjugated Fabs with the fluorophore Alexa Fluor 594 and used this reagent to "label" human embryonic kidney (HEK) cells that were transfected with TRAAK channels fused to green fluorescent protein (GFP) on their C terminus. Green HEK cells (i.e., those expressing TRAAK channels) were labeled with the fluorescent Fabs, whereas HEK cells that did not express TRAAK remained unlabeled (Fig. 2*B*). Thus, the Fab binds specifically to TRAAK channels on the surface of HEK cells. If we assume that the Fab can only bind to the helical cap in its

Author contributions: S.G.B. and R.M. designed research; S.G.B. and E.B.C. performed research; S.G.B. contributed new reagents/analytic tools; S.G.B. and R.M. analyzed data; and S.G.B. and R.M. wrote the paper.

The authors declare no conflict of interest.

This article is a PNAS Direct Submission.

Freely available online through the PNAS open access option.

Data deposition: The atomic coordinates have been deposited in the Protein Data Bank, www.pdb.org (PDB ID code 4I9W).

[1]To whom correspondence should be addressed. E-mail: mackinn@rockefeller.edu.

This article contains supporting information online at www.pnas.org/lookup/suppl/doi:10.1073/pnas.1218950110/-/DCSupplemental.

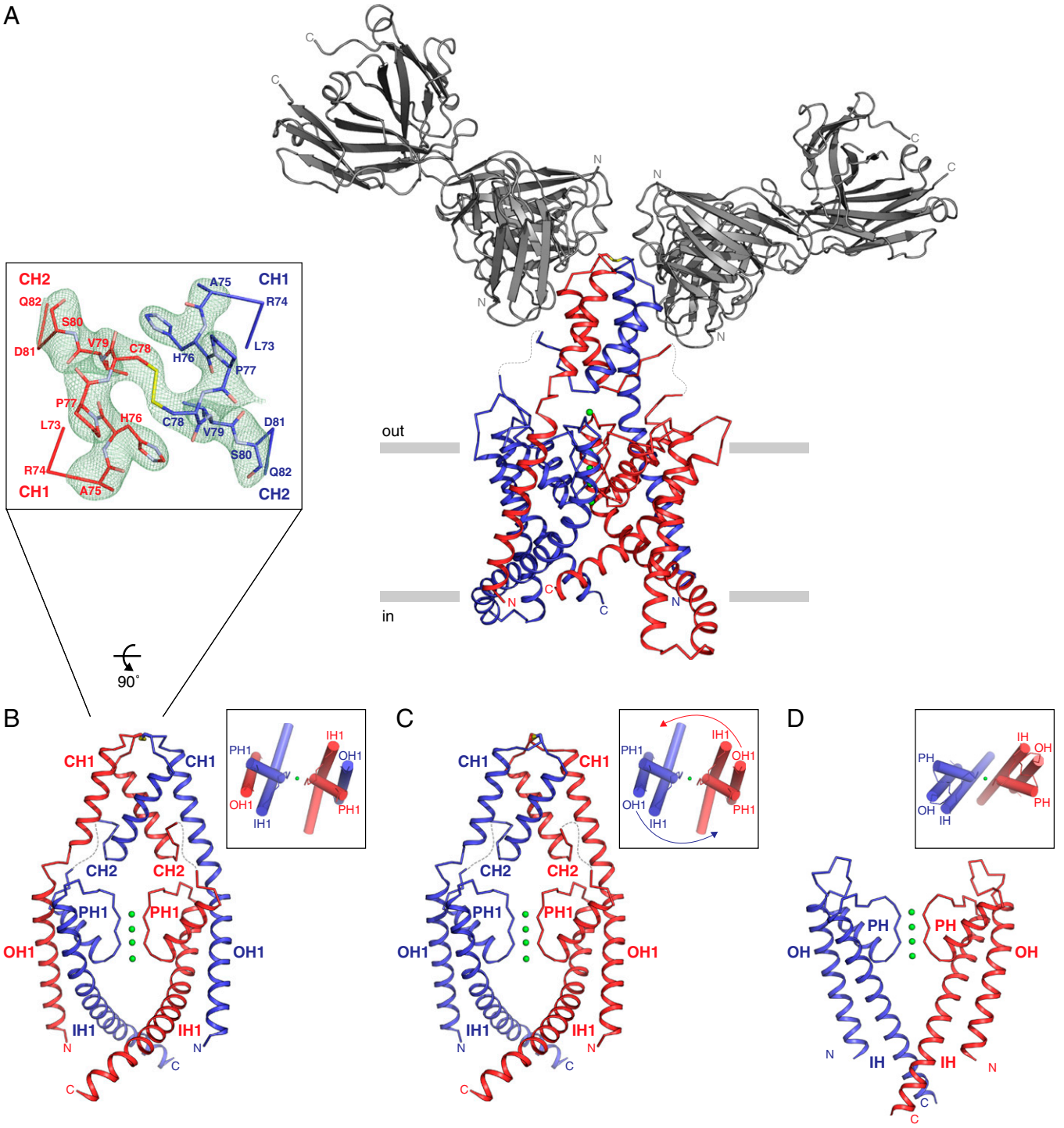

Fig. 1. Domain-swapped chain connectivity in a TRAAK-Fab complex structure. (*A*) View of the TRAAK-Fab structure from the membrane plane with the extracellular solution above. TRAAK is shown in ribbon representation, with one protomer chain subunit colored red and the second blue; potassium ions are shown as green spheres, and Fabs are shown as gray cartoons. The disulfide bond bridging the top of the helical cap is shown in stick representation with the cysteine sulfur colored yellow. Approximate boundaries of the membrane bilayer are indicated with gray bars. (*B*, *Left*) View of domain-swapped TRAAK from the membrane plane and rotated ~45° from *A*. The Fabs and second pore domain from each TRAAK subunit are removed for clarity. N and C termini, outer helix 1 (OH1), helical cap helix 1 (CH1), helical cap helix 2 (CH2), pore helix 1 (PH1), and inner helix 1 (IH1) are labeled. A loop connecting CH2 with PH1, for which no interpretable electron density was observed, is drawn as gray dashes. (*B*, *Right Inset*) View from the extracellular solution with helical cap removed. Helices are shown as cylinders. (*B*, *Upper Inset*) View of the top of the helical cap from above. Residues forming the connection between CH1 and CH2 are shown in stick representation inside a weighted F_o-F_c electron-density map (green mesh, contoured at 3.5 σ) calculated from a molecular replacement solution in which the illustrated region was omitted. (*C* and *D*) The original TRAAK structure (PDB ID code 3UM7) modeled without a domain swap (*C*) and the model K^+ channel KcsA [PDB ID code 1K4C (25)] from the same view as *B* (*D*). Viewed from the membrane plane, a right-handed migration of opposing OH1-CH1 units from the canonical K^+ channel architecture (indicated by arrows in the *Inset* to *C*) results in the domain-swapped chain connectivity observed in the TRAAK-Fab structure (*A* and *B*).

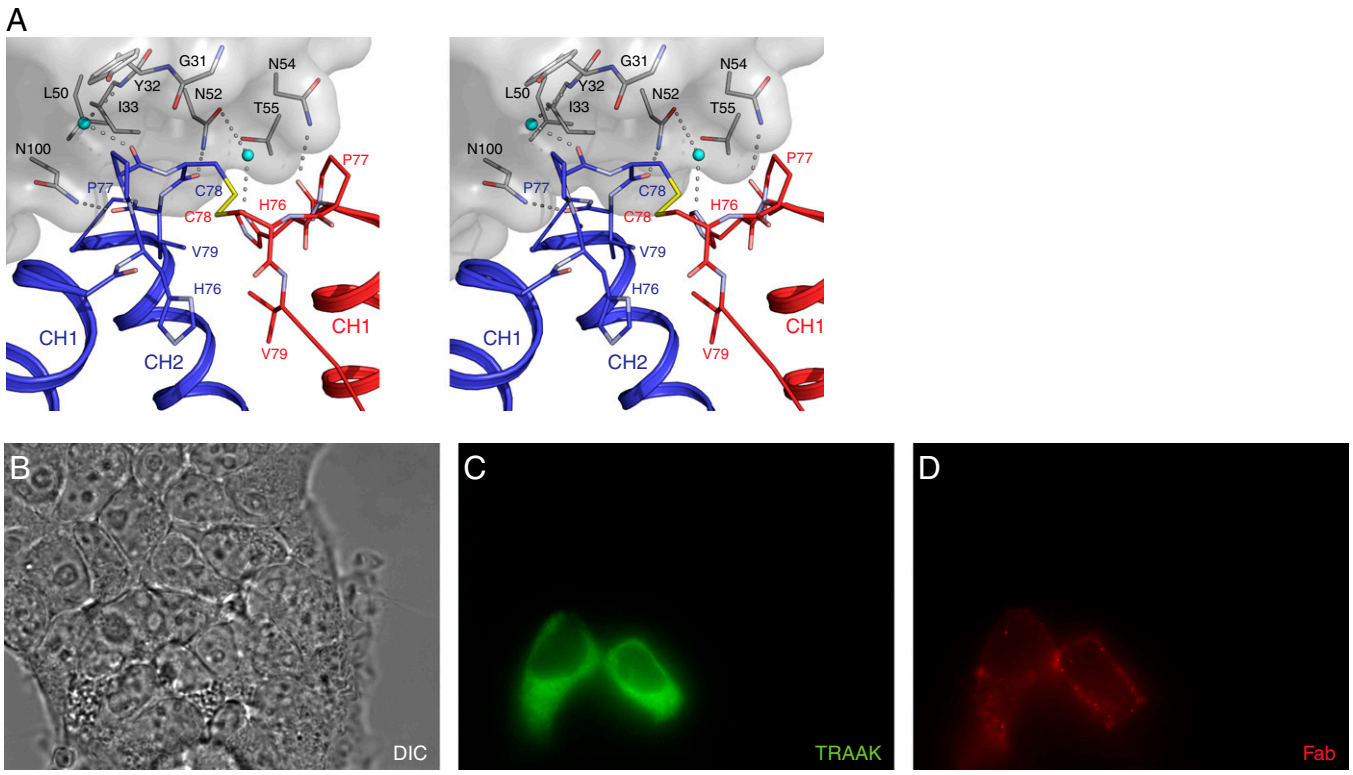

Fig. 2. TRAAK channels are domain-swapped in membranes. (*A*) Stereoview of the Fab interaction with the top of the domain-swapped helical cap. TRAAK is shown as ribbons and sticks colored as in Fig. 1. The variable domain from one Fab heavy chain is shown as a gray surface with residues that interact with the top of the domain-swapped helical cap shown as sticks. Two water molecules in the interface are shown as teal spheres. Hydrogen bonds are indicated with dashed lines. (*B*) Differential interference contrast (DIC) image of a group of live HEK cells. (*C*) Green fluorescence image from the same field of cells. Two of the cells express GFP-tagged TRAAK channels. (*D*) Red fluorescence image from the same field of cells. Only the two cells that express GFP-tagged TRAAK channels are labeled with Alexa Fluor 594-conjugated Fab. Data are representative of 54 total fields of view studied from five separate experimental repeats in which all cells that exhibited green fluorescence when transfected with TRAAK-EGFP also exhibited red fluorescence after incubation with Alexa Fluor 594-conjugated Fab. This is not attributable to nonspecific binding of the conjugated Fab because no cells were observed that exhibited red fluorescence in the absence of green fluorescence in TRAAK-EGFP–transfected cells. Additionally, no cells that exhibited green fluorescence when transfected with empty pCEH vector (and so expressed EGFP alone) also exhibited red fluorescence after incubation with AF594-conjugated Fab (in 30 total fields of view from five separate experimental repeats).

domain-swapped configuration [which we think is likely to be the case because of structural incompatibility between the Fab and a non–domain-swapped TRAAK channel (Fig. S2)], then we must conclude that at least some, if not all, of the channels in cell membranes exchange their outer helix 1-cap helix 1 unit between subunits. The answer to whether all of the channels or only a fraction of the population are domain-swapped will become clear as additional structures are determined in the future.

Even in retrospect, the diffraction data at 3.8 Å for the original model do not distinguish domain-swapped from non–domain-swapped models. However, given the greater accuracy of the higher-resolution model presented here, together with the fluorescent Fab labeling data on cell membranes, we suspect that the domain-swapped model is the generally correct model for TRAAK channels in cell membranes. What is the driving force behind the domain swap? The positions of atoms that make up the outer helix 1-cap helix 1 unit (amino acids 28–75) are the same in the models with and without the domain swap. Only four amino acids at the top of the helical cap (76–79) are different. Therefore, a preferred configuration adopted by these four amino acids must drive the domain swap. At present, we do not know whether the domain swap has any functional significance; however, it has obvious implications for protein folding and subunit assembly. After two independently folded subunits assemble, we imagine that the outer helix 1-cap helix 1 unit must migrate 180° counter clockwise (when viewed from the extracellular surface) around the channel's perimeter to adopt its domain-swapped location (Fig. 1*C*, *Inset*, and Movie S1).

The second observation, independent of the domain swap, is that one subunit has undergone conformational changes with respect to the other (Fig. 3*A*): the other subunit exhibits nearly the same conformation as both subunits of the original structure. A black copy of the transmembrane portion of the channel has been rotated 180° about the pore axis in Fig. 3*A* to highlight the conformational changes, which involve inner helix 2 and the selectivity filter to inner helix 2 connecting segment. More specifically, the intracellular C terminus of inner helix 2 is elevated, its extracellular N-terminal end has moved, and the connecting segment has undergone a substantial reorganization. These changes have two notable consequences. First, through new interactions formed between Phe^{272}, Val^{275}, Ile^{279}, and Leu^{283} on inner helix 2 and residues on inner helix 1 (particularly Leu^{151}) and pore helix 2 (particularly Leu^{236}), one of the prominent lateral openings that connects the ion pathway to the inner leaflet of the membrane has completely closed (Fig. 3 *B* vs. *C*). Second, interactions that tightly pack inner helix 2 against pore helix 1 are lost because of displacement of the extracellular end of inner helix 2 away from the ion conduction axis and a rotamer switch in the side chain of Trp^{262} (Fig. 3*D*).

We do not know whether these conformational changes are relevant to function; however, there is growing evidence that certain ion channels, including some K2P channels, do not close

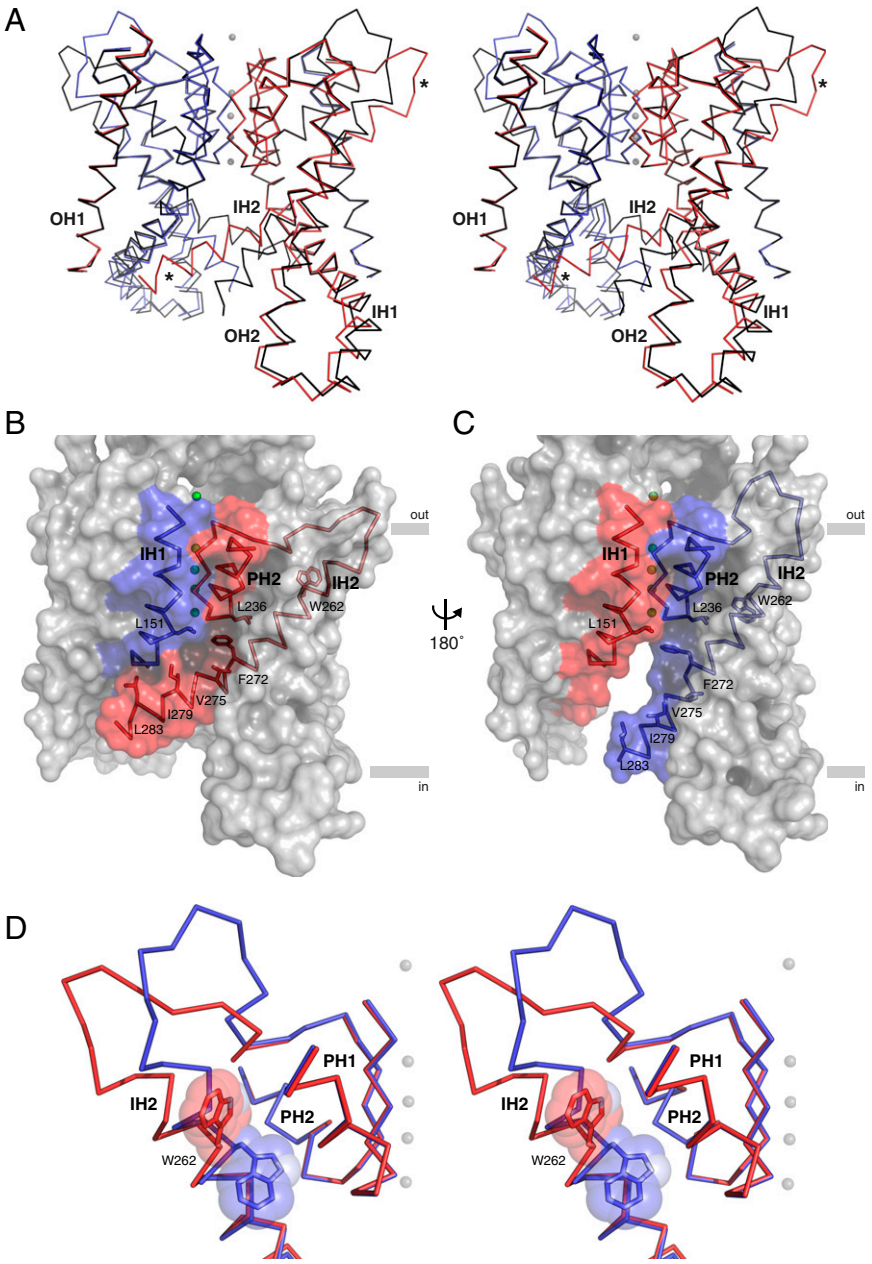

Fig. 3. Conformational changes in TRAAK inner helix 2 close a membrane-accessible side opening and remodel channel interactions around the selectivity filter. (*A*) Stereoview from the membrane plane of a superposition of two copies of the TRAAK channel structure from the current study in wire representation with helical caps removed. One channel, colored with one subunit red and the second blue, is in the same view as Fig. 1*A*. A second channel (colored black) has been rotated 180° about the pore axis. Outer helix 1 (OH1), inner helix 1 (IH1), outer helix 2 (OH2), and inner helix 2 (IH2) are labeled. Asterisks mark conformational differences between the IH2s. (*B* and *C*) Two views related by a 180° rotation about the pore axis from the membrane plane of the structure from the current study in surface and wire representation. IH1, pore helix 2 (PH2), and IH2 from one subunit are colored red and from the second subunit blue. Residues referred to in the text are labeled and shown as sticks. The conformational difference in the cytoplasmic half of IH2 between the subunits results in one closed (*B*) and one open (*C*) membrane side opening. Approximate boundaries of the lipid bilayer are indicated with gray bars. (*D*) Zoomed-in stereoview of a superposition of the extracellular side of IH2 from the two subunits. One channel subunit is colored red and the second is blue (as in *B*). Pore helix 1 (PH1), PH2, and IH2 are shown as wires, and Trp^{262} is shown as sticks with transparent surface. In the blue subunit [which has an open membrane side opening (*C*)], the extracellular end of IH2 including Trp^{262} packs against PH1. In the red subunit [which has a closed membrane side opening (*B*)], collapse and extension of the selectivity filter to IH2 connection, displacement of IH2 away from PH1, and a rotamer change of Trp^{262} results in a loss of the tightly packed interaction observed in the blue subunit around the selectivity filter.

an inner helical gate near the cytoplasmic entryway to the pore (6–10). Instead, it is thought that stimuli are somehow transmitted to the selectivity filter to turn conduction on or off. The conformational changes observed in the crystal structure could, in principle, transmit a signal across or from within the membrane via inner helix 2. This kind of stimulus transmission may be particularly relevant to TRAAK channels because they are known to gate in response to chemical or mechanical perturbation of the membrane (11–17). The selectivity filter is not perceptibly altered, but the rather significant structural changes around the filter associated with the movement of inner helix 2 might alter its dynamics or even its structure to an

imperceptibly small yet energetically significant degree that could influence ion conduction. A number of ion channel structures have now been found to contain side openings directly connecting the ion pathway to the membrane's lipid core (1, 2, 18, 19). In this case, the side opening is gated, the functional significance of which remains to be determined.

Materials and Methods

Cloning, Expression, and Purification of TRAAK. Cloning of *Homo sapiens* TRAAK (UniProt Q9NYG8-2) and heterologous expression in *Pichia pastoris* was described previously (1). The identical construct reported in the initial structure determination was used in this study. The crystallized construct is C-terminally truncated (by 119 aa), incorporates two mutations to remove N-linked glycosylation sites (N104Q/N108Q), and is expressed as a C-terminal PreScission protease-cleavable EGFP-His_{10} fusion protein (GE Healthcare). Human $TRAAK_{1–300(N104Q,N108Q)}$-SNS-LEVLFQ/GP-EGFP-H10 is referred to as TRAAK in the text for clarity.

Frozen *Pichia* cells grown in a fermenter (1) (typically 50 g) expressing TRAAK were disrupted by milling (model MM301; Retsch) five times for 3 min at 25 Hz. All subsequent purification steps were carried out at 4 °C. Cell powder was added to lysis buffer [50 mM Tris (pH 8.0), 150 mM KCl, 60 mM decyl-β-D-maltoside (DM) (Affymetrix), 0.1 mg/mL DNase 1, 1 μg/mL pepstatin, 1 μg/mL leupeptin, 1 μg/mL aprotinin, 10 μg/mL soy trypsin inhibitor, 1 mM benzamidine, and 1 mM phenylmethysulfonyl fluoride added immediately before use] at a ratio of 1 g of cell pellet per 4 mL of lysis buffer. Membranes were extracted for 3 h with gentle stirring followed by centrifugation at 35,000 × *g* for 45 min. Cobalt resin (Clontech) was added to the supernatant (1 mL of resin per 5 g of cell pellet) and stirred gently for 3 h. Resin was collected on a column and serially washed and eluted in IMAC buffer [50 mM Tris (pH 8.0), 150 mM KCl, 6 mM DM] with 10 mM, 30 mM, and 300 mM imidazole (pH 8.0). EDTA (pH 8.0) (1 mM final) and PreScission protease (~1:50 wt:wt) were added to the elution before incubation with gentle rocking overnight. Cleaved protein was concentrated (50-kDa molecular mass cutoff (MMCO)] and applied to a Superdex 200 column (GE Healthcare) equilibrated in SEC buffer [20 mM Tris (pH 8.0), 150 mM KCl, 1 mM EDTA, 4 mM *n*-decyl-β-D-maltopyranoside].

Antibody Generation and Purification. Monoclonal antibodies against TRAAK purified in dodecyl-β-D-maltopyranoside [as described (1)] were raised in mice using standard procedures. ELISA and Western blot analyses were used to identify initial positive clones. These positive clones were further tested for formation of stable antibody–TRAAK channel protein complexes by fluorescence-detection size-exclusion chromatography. Hybridoma supernatants (75 μL) were added to purified uncut TRAAK-EGFP (75 μL at 200 ng/μL in SEC buffer) and incubated at 4 °C for ≥10 min. A total of 100 μL of this reaction was injected on a Superdex 200 column run in SEC buffer, and clones that shifted TRAAK-EGFP retention time to an earlier-eluting, sharp, and monodisperse peak were selected for purification and cocrystallization trials.

Media supernatant (~100 mL) from hybridomas grown in disposable bioreactors (CELLine; BD) was dialyzed against two changes of 4 L of 10 mM Tris (pH 8.0), 10 mM KCl in 8-kDa-MMCO dialysis tubing overnight. Dialyzed samples were spun at 6,000 × *g*, and the supernatant was applied to a 5-mL Q-Sepharose column (GE Healthcare) equilibrated in 10 mM Tris (pH 8.0), 10 mM KCl. Antibodies were eluted during a gradient to 10 mM Tris (pH 8.0), 0.5 M KCl. Eluted antibodies were diluted to 2 mg/mL in PBS. Fab fragments were generated by reaction with papain (1:100 wt:wt) in PBS with 10 mM β-mercaptoethanol, 10 mM L-cysteine HCl, and 10 mM EDTA (pH 7.0) at 37 °C for 4 h. Cleaved antibodies were dialyzed against two changes of 4 L of 10 mM Tris (pH 8.0), 10 mM KCl in 8-kDa-MMCO dialysis tubing overnight. Dialyzed samples were spun at 6,000 × *g*, and the supernatant was applied to a 5-mL Q-Sepharose column equilibrated in 10 mM Tris (pH 8.0), 10 mM KCl. Fab fragments were collected in the flow-through, and low-salt fractions collected during gradient elution to 10 mM Tris (pH 8.0), 0.5 M KCl.

TRAAK-Fab Complex Purification and Crystallization. TRAAK-Fab complexes were prepared by incubating purified channel concentrated (50-kDa MMCO) to ~10 mg/mL with purified Fab concentrated (10-kDa MMCO) to ~30 mg/mL at a 1:2.5 molar ratio in SEC buffer for 10 min at 4 °C. TRAAK-Fab complex was separated from excess free Fab on a Superdex 200 column (GE Healthcare) equilibrated in SEC buffer. TRAAK-Fab complexes were concentrated (10-kDa MMCO) to 20–30 mg/mL for crystallization trials. Crystals of four different Fab complexes were obtained and screened for diffraction quality. Complexes with clone 13E9 gave the best-diffracting crystals and were used in this study. The protein sequence of the 13E9 Fab variable domains was determined by sequencing cDNA generated from hybridoma RNA (LakePharma).

Refined crystals were grown in drops of 0.25 μL of protein added to a 0.25-μL reservoir [50 mM Tris (pH 8.5), 200 mM $CaCl_2$, 27–30% (wt/vol) PEG400] in hanging drops over a 100-μL reservoir at 4 °C. Crystals appeared within 1 wk and grew to full size (~0.1 × 0.1 × 0.2 mm) in 2–6 wk. Crystals were harvested in cryoloops and directly frozen in liquid nitrogen.

Data Collection and Structure Determination. Data were collected at Advanced Photon Source (APS) Sector 23 Insertion Device Beamline B (23-ID-B) and processed with HKL2000 (20). Data from two crystals were scaled and merged to yield a complete dataset extending to 2.75-Å resolution. The structure was solved by molecular replacement with Phaser (21) using separate models for the 13E9 Fab constant and variable domains generated from the crystal structure of 33H1 (22) with complementarity-determining regions removed and side chains trimmed to the last common atom. Two copies of each constant and variable domain were located in the asymmetric unit. Phaser was used to locate one TRAAK channel from which the helical cap and inner helix 2s were removed. Starting phases were of sufficient quality to generate readily interpretable electron density for the regions omitted in the molecular replacement models. The structure was manually modeled by iterative building in Coot (23) and refinement in Refmac (24). Twofold local non-crystallographic symmetry and jelly-body restraints were used throughout refinement and three translation/libration/screw (TLS) groups per protein chain were incorporated during the final rounds of refinement that converged to an R_{free} = 23.6% with excellent geometry (Table S1). The final model consists of TRAAK residues 28–103 and 110–286 in protomer A, residues 28–105 and 110–284 in protomer B, two copies each of 13E9 Fab light chain residues 1–211 and heavy chain residues 1–129 and 136–217, five K^+ ions, two Ca^{2+} ions, and 153 water molecules. We note that the unmodeled loop region in TRAAK could, in principle, connect helical cap helix 2 to pore helix 1 from either subunit and, thus, result in an alternative non–domain-swapped model to the domain-swapped model we present. However, the loop is not long enough to wrap around the outside of the channel, and the structure does not leave sufficient space between the helical cap and mouth of the ion-conduction pore to allow threading of the loops underneath the helical cap. Thus, we are confident in the connectivity between cap helix 2 and pore helix 1 indicated by the dashes in Fig. 1.

Fab Fluorescent-Labeling Experiments. Purified 13E9 Fab was dialyzed against two changes of 4L of PBS in 8-kDa-MMCO dialysis tubing overnight before fluorophore conjugation. Freshly prepared 10 mg/mL Alexa Fluor 594 carboxylic acid succinimidyl ester (Invitrogen) in DMSO was added to 2 mg/mL 13E9 Fab in PBS and 100 mM $NaHCO_3$ (pH 8.3) at a 1:20 weight ratio and incubated with gentle rocking at 25 °C for 1 h. Conjugated Fab was separated from excess fluorophore on a 5-mL HiTRAP desalting column (GE Healthcare) run in PBS. Degree of labeling was determined to be ~6 mol of Alexa Fluor 594 per 1 mol of Fab spectroscopically. Conjugated Fab was concentrated to 2 mg/mL and stored at 4 °C.

The identical TRAAK construct used in crystallization was cloned into a pCEH vector to generate a C-terminally tagged $TRAAK_{1–300(N104Q,N108Q)}$-SNSAVDAGLVPRGSAAA-EGFP-$H_{10}$ construct for mammalian cell expression that has been shown previously to generate functional TRAAK channels (1). HEK293T cells (ATCC) were cultured in DMEM with 10% FBS, 2 mM L-glutamine, 100 U/mL penicillin, and 100 μg/mL streptomycin (Gibco). Cell stocks were maintained in plastic dishes and split into collagen-coated glass bottom dishes (Mattek) 24 h before transfection using FugeneHD (Promega) following the manufacturer's protocol. Media were changed after 24 h. Thirty hours after transfection, cells were washed twice with culture media; incubated for 30 min in culture media with conjugated Fab at a 1:1,000 dilution; washed four times with culture media and twice with 10 mM Hepes (pH 7.3), 3 mM $MgCl_2$, 1 mM $CaCl_2$, 15 mM KCl, and 135 mM NaCl; and immediately imaged. Imaging was performed with a Nikon Eclipse Ti-S inverted microscope with 100× oil immersion objective using FITC-HYQ and Y-2E/C filter sets for EGFP and Alexa Fluor 594 epifluorescence, respectively.

ACKNOWLEDGMENTS. We thank Ruslan Sanishvili, Stephen Corcoran, and the staff at Beamline 23-ID-B at the APS for assistance at the synchrotron; Josefina del Mármol for advice on performing imaging experiments; the Memorial Sloan-Kettering Cancer Center and Rockefeller University Bi-Institutional Monoclonal Antibody Core Facility for assistance with monoclonal antibody generation; and members of the laboratory of R.M. for helpful discussions. S.G.B. is a Howard Hughes Medical Institute fellow of the Helen Hay Whitney Foundation, and R.M. is an investigator of the Howard Hughes Medical Institute.

1. Brohawn SG, del Mármol J, MacKinnon R (2012) Crystal structure of the human K2P TRAAK, a lipid- and mechano-sensitive K+ ion channel. *Science* 335(6067):436–441.
2. Miller AN, Long SB (2012) Crystal structure of the human two-pore domain potassium channel K2P1. *Science* 335(6067):432–436.
3. del Camino D, Yellen G (2001) Tight steric closure at the intracellular activation gate of a voltage-gated K(+) channel. *Neuron* 32(4):649–656.
4. Jiang Y, et al. (2002) The open pore conformation of potassium channels. *Nature* 417(6888):523–526.
5. Enyedi P, Czirják G (2010) Molecular background of leak K+ currents: Two-pore domain potassium channels. *Physiol Rev* 90(2):559–605.
6. Bagriantsev SN, Clark KA, Minor DL (2012) Metabolic and thermal stimuli control K2P2.1 (TREK-1) through modular sensory and gating domains. *EMBO J* 31(15):3297–3308.
7. Bagriantsev SN, Peyronnet R, Clark KA, Honoré E, Minor DL, Jr. (2011) Multiple modalities converge on a common gate to control K2P channel function. *EMBO J* 30(17): 3594–3606.
8. Piechotta PL, et al. (2011) The pore structure and gating mechanism of K2P channels. *EMBO J* 30(17):3607–3619.
9. Cohen A, Ben-Abu Y, Hen S, Zilberberg N (2008) A novel mechanism for human K2P2.1 channel gating. Facilitation of C-type gating by protonation of extracellular histidine residues. *J Biol Chem* 283(28):19448–19455.
10. Zilberberg N, Ilan N, Goldstein SA (2001) KCNKØ: Opening and closing the 2-P-domain potassium leak channel entails "C-type" gating of the outer pore. *Neuron* 32(4): 635–648.
11. Fink M, et al. (1998) A neuronal two P domain K+ channel stimulated by arachidonic acid and polyunsaturated fatty acids. *EMBO J* 17(12):3297–3308.
12. Kang D, Choe C, Kim D (2005) Thermosensitivity of the two-pore domain K+ channels TREK-2 and TRAAK. *J Physiol* 564(Pt 1):103–116.
13. Maingret F, Fosset M, Lesage F, Lazdunski M, Honoré E (1999) TRAAK is a mammalian neuronal mechano-gated K+ channel. *J Biol Chem* 274(3):1381–1387.
14. Maingret F, Patel AJ, Lesage F, Lazdunski M, Honoré E (2000) Lysophospholipids open the two-pore domain mechano-gated K(+) channels TREK-1 and TRAAK. *J Biol Chem* 275(14):10128–10133.
15. Lesage F, Maingret F, Lazdunski M (2000) Cloning and expression of human TRAAK, a polyunsaturated fatty acids-activated and mechano-sensitive K(+) channel. *FEBS Lett* 471(2-3):137–140.
16. Kim Y, Bang H, Gnatenco C, Kim D (2001) Synergistic interaction and the role of C-terminus in the activation of TRAAK K+ channels by pressure, free fatty acids and alkali. *Pflugers Arch* 442(1):64–72.
17. Chemin J, et al. (2005) Lysophosphatidic acid-operated K+ channels. *J Biol Chem* 280(6):4415–4421.
18. Payandeh J, Scheuer T, Zheng N, Catterall WA (2011) The crystal structure of a voltage-gated sodium channel. *Nature* 475(7356):353–358.
19. Zhang X, et al. (2012) Crystal structure of an orthologue of the NaChBac voltage-gated sodium channel. *Nature* 486(7401):130–134.
20. Minor W, Cymborowski M, Otwinowski Z, Chruszcz M (2006) HKL-3000: The integration of data reduction and structure solution—from diffraction images to an initial model in minutes. *Acta Crystallogr D Biol Crystallogr* 62(Pt 8):859–866.
21. McCoy AJ, et al. (2007) Phaser crystallographic software. *J Appl Cryst* 40(Pt 4): 658–674.
22. Jiang Y, et al. (2003) X-ray structure of a voltage-dependent K+ channel. *Nature* 423(6935):33–41.
23. Emsley P, Lohkamp B, Scott WG, Cowtan K (2010) Features and development of Coot. *Acta Crystallogr D Biol Crystallogr* 66(Pt 4):486–501.
24. Murshudov GN, et al. (2011) REFMAC5 for the refinement of macromolecular crystal structures. *Acta Crystallogr D Biol Crystallogr* 67(Pt 4):355–367.
25. Zhou Y, Morais-Cabral JH, Kaufman A, Mackinnon R (2001) Chemistry of ion coordination and hydration revealed by a K+ channel-Fab complex at 2.0 A resolution. *Nature* 414(6859):43–48.